



A modeling method for predicting friction torque of the preload double-nut ball screw based on thermal elastohydrodynamic lubrication

Jiajia Zhao¹ · Baobao Qi^{2,3} · Xianchun Song¹ · Hongkui Jiang¹ · Pengfei Dong¹

Received: 5 May 2022 / Accepted: 8 June 2022 / Published online: 2 July 2022
© The Author(s), under exclusive licence to Springer-Verlag London Ltd., part of Springer Nature 2022

Abstract

Ball screw has become a key functional component commonly used in actuators of high-end machine tools because of its high transmission efficiency, low environmental impact, and strong universality of working conditions. For the high-precision ball screw, the proper and constant preload is the premise to maintain the transmission accuracy and reliable dynamic characteristics of the ball screw. The direct measurement of the preload is difficult to be achieved. Usually, the preload of the ball screw is indirectly determined by the friction torque of the ball screw under no-load condition. In previous studies, the influence of lubrication on friction torque of the ball screw was not considered, and the influence of operating conditions on performance of lubricant was ignored, and the influence of contact elastic hysteresis effect and the sliding friction effect was not considered, which seriously affected the modeling accuracy of friction torque for the ball screw. Therefore, on the basis of considering the contact elastic hysteresis friction and the sliding friction of the ball screw in the paper, a calculation model of friction torque for the ball screw based on the coupling of the ball load distribution and the thermal elastohydrodynamic lubrication is proposed. The mechanism of different friction terms on the friction torque of the ball screw is analyzed, and the coupling relationship among preload, rotational speed, and friction torque is established. The experimental results show that the proposed method, which the ball load distribution, the thermal elastohydrodynamic lubrication, the elastic hysteresis, and the sliding friction are comprehensively considered, has a good reference significance for improving the internal preload and predicting the precision degradation of the ball screw.

Keywords Ball screw · Thermal elastohydrodynamic lubrication · Friction torque · Elastic hysteretic friction · Sliding friction

1 Introduction

With the development of numerical control machine tools to the direction of high reliability, high precision, and extreme manufacturing, the high-end numerical control machine

tools are in urgent need of high reliability core executive components. Ball screws have become key functional components of actuators in high-end machine tools due to its characteristics of high transmission efficiency, low environmental impact, and strong universality of working conditions [1–3]. As shown in Fig. 1, the double-nut ball screw is mainly made up of the screw, the preload nut, the work nut, the reverser, and the spacer. In order to eliminate the reverse clearance of ball screw and improve its transmission accuracy, the different preload should be applied in application fields [4, 5]. Although the transmission characteristics of the ball screw can be improved by adjusting the large preload, the increasing preload causes to the increase of the contact load between the ball and the raceway. The contact friction of the ball screw is aggravated due to the increasing load, which has a negative impact on the precision life of the ball screw. In addition, the preload is the internal force

✉ Baobao Qi
qibaobao@jlu.edu.cn

✉ Xianchun Song
songxch@sdjzu.edu.cn

¹ School of Mechanical and Electrical Engineering, Shandong Jianzhu University, Jinan, Shandong 250101, China

² Key Laboratory of CNC Equipment Reliability, Ministry of Education, Changchun, Jilin 130022, China

³ School of Mechanical and Aerospace Engineering, Jilin University, Changchun, Jilin 130022, China

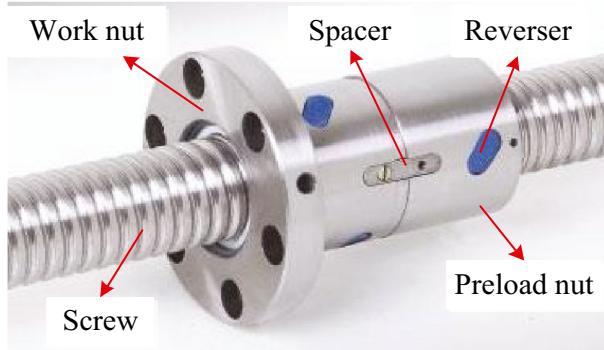


Fig. 1 The mechanism of the double-nut ball screw

of the ball screw, which is not easy to be measured directly after assembly. In general, the preload of the ball screw is obtained indirectly through the calculation of the measured no-load friction torque [6, 7]. Therefore, the accurate calculation of friction torque is very important for the design process of the ball screw.

As a closed circulation system, it is difficult for the ball screw to experimentally study the dynamic performance of internal balls, and several researches have been carried out to investigate the motion state of balls within the ball screw mechanism [8]. It is obviously known that the friction torque generated in the ball screw depends on the applied load and redistributed state of all balls. Lin et al. [9] established the vector space coordinate system of the ball screw and analyzed the influence of contact deformation of moving ball on sliding characteristics based on transformation of the space coordinate system. On this basis, Hu et al. [10] further improved representation method of the vector space coordinate system for the ball screw and established the kinematic model of the ball screw by using homogeneous transformation matrix. Considering the change of contact angle and contact elastic deformation of the ball screw, Wei and Lai [11, 12] analyzed the sliding behavior generated by the two contact areas and the influence of the friction coefficient or the normal force on its motion characteristics of the ball screw. It is assumed that the contact load and motion states of all balls in the closed raceway are completely consistent. Therefore, there will be some deviation in the application of the model in actual working conditions. The accurate calculation of load distribution is helpful to guide the innovative design and selection of the ball screw. Some researchers [13, 14] analyzed the load distribution under axial load by simplifying the screw and nut of the ball screw into a two-dimensional plane based on the marking tracking method of displacement field and the photoelastic image of stress field. The simplified setting misdefines the three-dimensional force–displacement interaction in the practical application of the ball screw. Yoshida et al. [15, 16] proposed the calculation formula of ball stress

distribution and rolling characteristics through numerical theoretical analysis and analyzed the change of the dynamic contact stiffness for the feed system in the process of circular operation.

On the assumption that the contact angle between the ball and the raceway is equal and unchanged after being loaded, Mei et al. [17] proposed the ball load distribution model considering the manufacturing error under axial load conditions and proposed that the consistency of the ball load distribution can be improved by changing the pitch. On the basis of Mei' model, Xu et al. [18] analyzed the influence of contact angle on the ball load distribution, and Liu et al. [19] further made a comparative analysis on the ball load distribution. The lateral deformation and torsional deformation of the ball screw were ignored in the above studies, and only the axial deformation of the ball screw was considered. Zhen and An [20] proposed the analysis method of the ball load distribution for the ball screw under the combined action of axial and radial loads and calculated the contact stress and fatigue life through mechanical analysis. In order to discuss the influence of lateral deformation for the ball screw, Lin and Okwudire [21, 22] studied the coupling relations of axial, torsional, and lateral deformation for the ball screw under the assumption of equal contact angle and analyzed the influence of coupling contact deformation and manufacturing geometric error on ball load distribution. Zhou et al. [23] proposed a modified load distribution model to obtain the critical axial load of the double-nut ball screw with and without adding the elastic element.

The relationship between the preload and the no-load friction torque of the ball screw mainly used in the field is an empirical formula, which was proposed by NSK company in 2003 [24]. However, the measuring conditions of the no-load friction torque are not described by the empirical formula, and the influence of lead angle for the screw on the no-load friction torque is only considered. The other parameters affecting the no-load friction torque, such as contact angle and friction coefficient, are not reflected in the empirical formula. Many relevant studies on the friction torque of the ball screw were proposed by researchers. Xu et al. [25] established the calculation method of the friction torque for the ball screw based on the rolling-sliding contact theory and analyzed the influence of rolling-sliding parameters and contact parameters on the friction torque. Zhou et al. [26] proposed a calculation method of the friction torque for all balls considering the changes of contact angle and lead angle for the ball screw under the action of preload. Considering the influence of lubrication and temperature rise, Bertolino et al. [27] simulated the friction torque of the ball screw based on multi-rigid body dynamics model. Zhao et al. [28] installed a new grinding tool on a specially designed friction torque tester to dynamically control the rotation of the screw and monitor the change of the friction torque of the ball

screw. The authors established a lumped parameter dynamic model of the double-nut preloaded ball screw [29, 30] in which evolved in a more detailed three-dimensional multi-body dynamic model [27], capable to describe the motion state of all balls for the ball screw mechanism. The focus has been put on the punctual contact between the ball and the raceway in the consideration of grease lubrication. Some fault evolution models have been proposed to study the influence on the overall performance of the ball screw.

The structure of our paper can be expressed as follows: In Sect. 2, the coupled analysis of kinematic model for the ball screw is established, and the entrainment rate, the slip rate, and the roll-slip ratio of the contact micro-zone are obtained to analyzed the Reynolds equation by using the substitution method of parameters. Then, the film thickness and the pres-

2 Analysis of thermal elastohydrodynamic lubrication

2.1 Analysis of kinematics

Taking the kinematics analysis of a single ball as an example, the contact state and the relative coordinate system between the ball and the raceway are shown in Fig. 2. In the study of the thermal elastohydrodynamic lubrication, only the velocity of the elliptic contact point in the X direction is considered. Based on the previous research discussion and analysis, the velocity of the contact micro-zone between the ball and the raceway can be obtained [31, 32]. Therefore, the linear velocities of contact point for the ball screw can be expressed as follows:

$$U_{sb} = \sqrt{(r_m(\dot{\theta} - \dot{\Omega})/\cos\lambda - r_b(w_b \cos\beta_i - w_n \sin\beta_i) + r_m \dot{\Omega} \cos\lambda)^2 + (r_m \dot{\Omega} \sin\lambda - r_b w_t \cos\beta_i)^2 + (r_b w_t \sin\beta_i)^2} \tag{1}$$

$$U_{nb} = \sqrt{(r_m(\dot{\theta} - \dot{\Omega})/\cos\lambda + r_b(w_b \cos\beta_i - w_n \sin\beta_i) + r_m \dot{\Omega} \cos\lambda)^2 + (r_m \dot{\Omega} \sin\lambda + r_b w_t \cos\beta_i)^2 + (r_b w_t \sin\beta_i)^2} \tag{2}$$

sure distribution of lubricant is analyzed, and the viscosity, density, and load equations of lubricant are established. Finally, the energy heat convection equation of contact solids (ball and raceway) is analyzed to solve the thermal elastohydrodynamic lubrication in the contact zone. In Sect. 3, the calculation method of the viscous friction force, the elastic hysteresis friction, and the slipping friction force is obtained. The ball load distribution of the double-nut ball screw under the preload is studied, and the calculation method of the friction torque for the ball screw considering the viscous friction, the elastic hysteresis friction, and the sliding friction is proposed. In Sect. 4, a novel test bench measuring friction torque of the ball screw is designed. The proposed prediction method of the friction torque based on the thermal elastohydrodynamic lubrication is validated. The friction torque under different preload and rotational speed of the ball screw is measured during operation test, and there is a comparative analysis including the experimental results, the proposed model, NSK model, and Zhou’s model to verify the prediction accuracy of the proposed model. In Sect. 5, the thermal elastohydrodynamic lubrication performance of contact point between ball and raceway is analyzed. The viscous friction, the elastic hysteresis friction, and the sliding friction of the ball screw at different speeds are studied respectively. The friction torque under different sliding friction coefficient and different environment viscosity caused by different lubricating oil temperatures is compared, and the friction torque of the ball screw under different preload is analyzed.

The linear velocity of contact point between the ball and the screw raceway at the side of the screw can be expressed as:

$$U_s = \dot{\Omega} \sqrt{(r_m - r_b \cos\beta_i)^2 + r_b \sin^2\beta_i \sin^2\lambda} \tag{3}$$

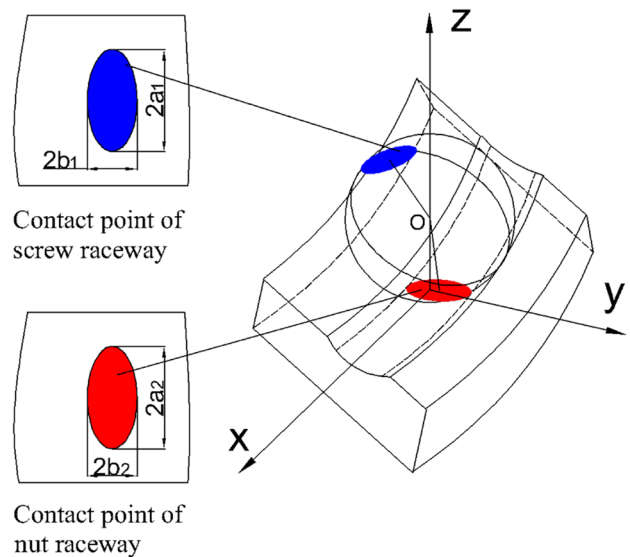


Fig. 2 Contact area between the ball and the raceway

The linear velocity of contact point between the ball and the nut raceway at the nut side can be expressed as:

$$U_n = r_m \dot{\Omega} \tan \lambda \tag{4}$$

where the parameters in Eqs. (1)–(4) are defined in Zhao et al. [31]. The entrainment rate at the contact micro-area is $U_{Le} = (U_L + U_{Lb})/2$ ($L = s$ and n represent the contact side of the screw and the nut, respectively). The slip rate at the contact micro-area is $U_{Lr} = U_L - U_{Lb}$, and the slip-roll ratio of the contact micro-area is $S_L = U_{Lr}/U_{Le}$.

2.2 Analysis of film thickness and pressure distribution

When the thermal effect of lubricating oil film is considered, the viscosity and density of lubricating oil film are different in the direction of oil film thickness. The Reynolds equation of the elastohydrodynamic lubrication considering the thermal effect can be written as:

$$\frac{\partial}{\partial x} \left(\frac{\rho h^3}{\eta} \cdot \frac{\partial p}{\partial x} \right) + \frac{\partial}{\partial y} \left(\frac{\rho h^3}{\eta} \cdot \frac{\partial p}{\partial y} \right) = 12U_{Le} \cdot \frac{\partial(\rho h)}{\partial x} \tag{5}$$

Since the nominal friction torque in the paper represents the average friction torque on the effective stroke of the ball screw, the manufacturing error and the surface roughness of the raceway have average effect when the average friction torque is solved. Therefore, the influence of the manufacturing error and the surface roughness on film thickness can be ignored, and the film thickness can be expressed as:

$$h(x, y) = h_0 + \frac{x^2}{2R_x} + \frac{y^2}{2R_y} \tag{6}$$

where h_0 is the oil film thickness at the center of the elliptic contact point, R_x and R_y are the equivalent radius of the contact point in the x and y directions, respectively, $R_x = R_{11} \cdot R_{21} / (R_{11} + R_{21})$, $R_y = R_{12} \cdot R_{22} / (R_{12} + R_{22})$, as shown in Fig. 3.

2.3 Analysis of viscosity, density, and load for lubricant

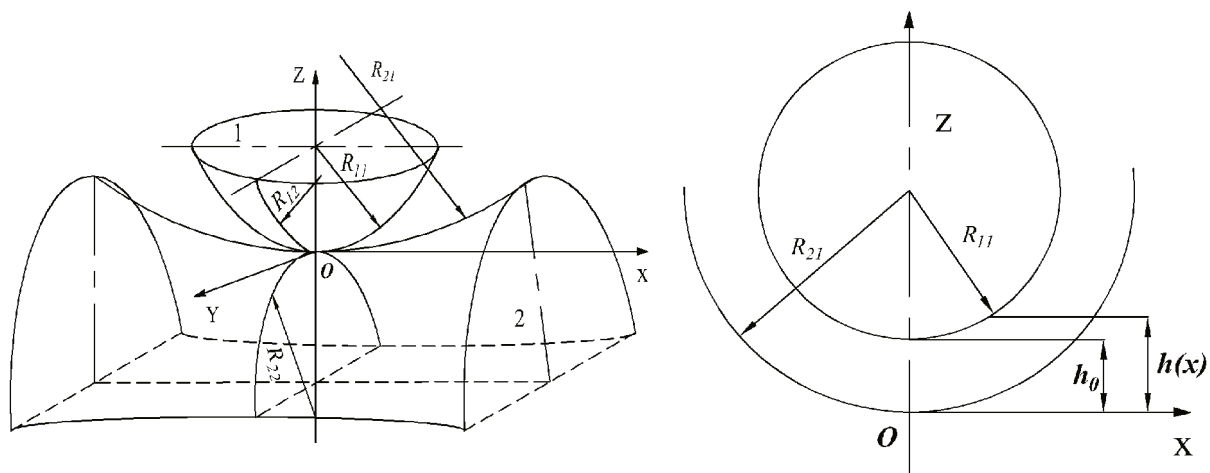
The viscosity of lubricant based on the Roelands viscous-pressure formula can be written as:

$$\eta = \eta_0 \exp \left\{ (\ln \eta_0 + 9.67) \cdot \left[(1 + 5.1 \times 10^{-9} p)^{z_0} \cdot \left(\frac{T - 138}{T_0 - 138} \right)^{-s_0} - 1 \right] \right\} \tag{7}$$

The temperature coefficient is $s_0 = \gamma(T_0 - 138) / (\ln \eta_0 + 9.67)$; γ is the viscosity-temperature coefficient; T_0 is the initial environmental temperature. The pressure coefficient is $z_0 = \alpha / 5.1 \times 10^{-9} (\ln \eta_0 + 9.67)$; The initial environmental viscosity is $\eta_0 = 4.83 \times 10^{-5} \exp \{ 1045.31 / (T_0 - 183.19) \}$, α is the viscous-pressure coefficient. Based on the Dowson-Higginson density-pressure formula, the density of lubricant can be expressed as:

$$\rho = \rho_0 \left[1 + \frac{0.6 \times 10^{-9} p}{1 + 1.7 \times 10^{-9} p} - D_0(T - T_0) \right] \tag{8}$$

In order to solve Eq. (5), the contact boundary conditions of Reynolds equation (shown in Fig. 4) can be expressed as:



(a) Principal curvature radius of contact point (b) Film thickness of contact point in the x direction

Fig. 3 Film thickness of contact point for the ball screw. a Principal curvature radius of contact point. b Film thickness of contact point in the x direction

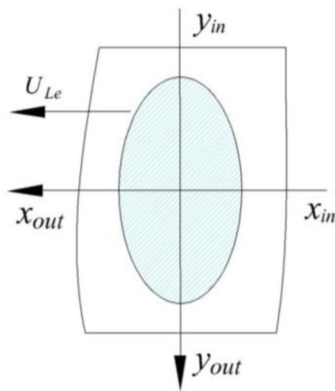


Fig. 4 The elliptic contact area of thermal elastohydrodynamic lubrication

$$\begin{cases} p(x_{in}, y) = p(x_{out}, y) = 0 \\ p(x, y_{in}) = p(x, y_{out}) = 0 \\ p(x, y) \geq 0 (x_{in} \leq x \leq x_{out}, y_{in} \leq y \leq y_{out}) \end{cases} \quad (9)$$

The thermal elastohydrodynamic lubrication analysis of the ball screw is carried out under given preload conditions, and the load balance equation of oil film pressure in micro-contact area can be obtained:

$$Q_j = \iint p(x, y) dx dy ; j = 1, 2, \dots, N \quad (10)$$

2.4 Analysis of energy heat convection

For solving the thermal elastohydrodynamic lubrication in the contact area, it is necessary to consider the influence of the thermal effect in analyzing the temperature field, which is usually resolved according to the heat conduction equation

of contact solids (ball and raceway), oil film energy equation, and lubrication boundary conditions. The energy control equation of oil film considering the thermal convection and conduction can be written as follows:

$$c\rho \left(u \frac{\partial T}{\partial x} + v \frac{\partial T}{\partial y} + w \frac{\partial T}{\partial z} \right) = k \frac{\partial^2 T}{\partial z^2} - \frac{T}{\rho} \frac{\partial \rho}{\partial T} \left(u \frac{\partial p}{\partial x} + v \frac{\partial p}{\partial y} \right) + \eta \left[\left(\frac{\partial u}{\partial z} \right)^2 + \left(\frac{\partial v}{\partial z} \right)^2 \right] \quad (11)$$

The velocity continuity control equation of the elliptic point contact can be expressed as:

$$\frac{\partial(\rho u)}{\partial x} + \frac{\partial(\rho v)}{\partial y} = \frac{\partial(\rho w)}{\partial z} \quad (12)$$

The temperature boundary conditions of the lower and upper surfaces (between the ball and the screw raceway or the nut raceway) for the elliptic contact surface can be expressed as follows:

$$\begin{cases} T(x, y, 0) = \frac{k}{\sqrt{\pi \rho_1 c_1 k_1 u_1}} \int_{-\infty}^x \frac{\partial T}{\partial z} \Big|_{x_j, y_j, 0} \frac{ds}{\sqrt{x-s}} + T_0 \\ T(x, y, h) = \frac{k}{\sqrt{\pi \rho_2 c_2 k_2 u_2}} \int_{-\infty}^x \frac{\partial T}{\partial z} \Big|_{x_j, y_j, h} \frac{ds}{\sqrt{x-s}} + T_0 \end{cases} \quad (13)$$

where the relevant parameters can be defined in Table 1.

3 Friction torque model of the ball screw

3.1 Analysis of viscous friction force

Under the condition of the thermal elastohydrodynamic lubrication, the lubricating oil film is formed at the contact

Table 1 Structure and lubrication parameters of the ball screw

Structure parameters	Value	Lubrication parameters	Value
Nominal radius, r_m , (mm)	20	Environmental density, ρ_0 , (kg/m ³)	970
Ball diameter, d_b , (mm)	4.763	Densities of ball and raceway, ρ_1, ρ_2 , (kg/m ³)	7870
Initial contact angle, β_0 , (°)	45	Environmental viscosity, η_0 , (Pas)	0.033
Raceway radius r_s, r_n , (mm)	2.477	Specific heat of lubricant, c , (J/(kg K))	1910
Lead angle, λ , (°)	3.64	Specific heat of interface, c_1, c_2 , (J/(kg K))	450
Ball number, z	86	Thermal conductivity of lubricant, k , (W/m K)	0.14
Rows × turns, $N \times I$	3 × 1	Thermal conductivity of interface, k_1, k_2 , (W/m K)	46
Lead, L_p , (mm)	8	Viscosity-pressure coefficient, γ , (Pa ⁻¹)	1.85 × 10 ⁻⁸
Poisson's ratio, μ_1, μ_2	0.3	Viscosity-temperature coefficient, α , (K ⁻¹)	0.032
Young's modulus, E_1, E_2 , (GPa)	205	Initial temperature, T_0 , (K)	303
Useful stroke, L_s , (mm)	1000	Autocorrelation length, L_x, L_y , (μm)	50
Lubrication mode	Oil	Density-temperature coefficient, D , (K ⁻¹)	-0.00065

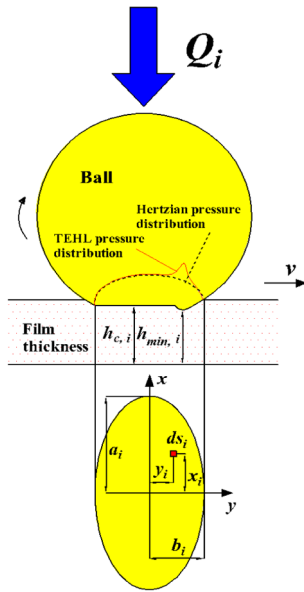


Fig. 5 Pressure distribution and film thickness of contact point

ellipse between the ball and the raceway, as shown in Fig. 5. The shear stress between a single ball and the contact surface in the lubricating area of oil film can be expressed as:

$$\tau = \eta \frac{\partial u}{\partial z} \tag{14}$$

The viscous friction force generated by a single ball on the contact ellipse of the raceway can be expressed as:

$$F_{v,i}(x_i, y_i) = \frac{\eta_i \partial u_i}{\partial h_i} \int_{-a_i}^{+a_i} \int_{-b_i}^{+b_i} \sqrt{1 - \frac{x_i^2}{a_i^2} - \frac{y_i^2}{b_i^2}} dy_i dx_i = \frac{\eta_i \partial u_i \pi a_i b_i}{\partial h_i} \tag{15}$$

Considering all balls distributed in the ball screw, the total viscous friction force can be written as:

$$F_v = \sum_{i=1}^Z \frac{\eta_i \partial u_i \pi a_i b_i}{\partial h_i} \tag{16}$$

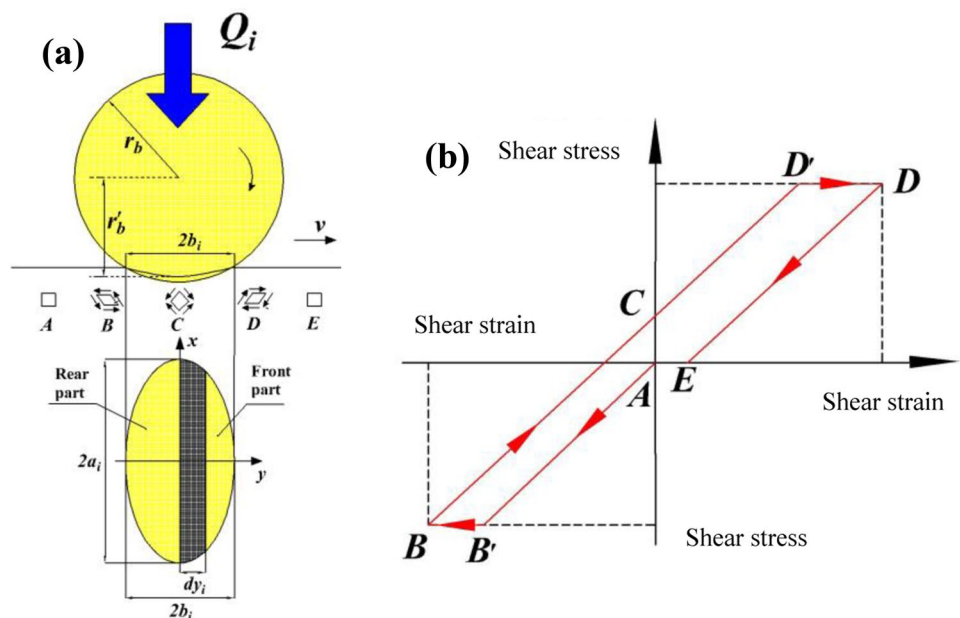
3.2 Analysis of elastic hysteresis friction

Figure 6a shows the Hertz contact ellipse of the ball under the given contact load Q_i . The contact stress distribution of the contact ellipse for the i th ball can be expressed as:

$$q_i(x_i, y_i) = \frac{3Q_i}{2\pi a_i b_i} \sqrt{1 - \frac{x_i^2}{a_i^2} - \frac{y_i^2}{b_i^2}} \tag{17}$$

The ball is spirally rolling along the raceway in the high stress state, which causes local deformation on the contact surface and the plastic shear stress–strain cycle on the secondary surface, as shown in Fig. 6a, b. For the ball rolling forward, the stress and strain states vary from A to B to C until varying to E. The sub-surface contact element deforms elastically from A to B' until the yield stress is reached. At this point, the strain continues to increase to a maximum at point B, and the contact element is subjected

Fig. 6 a Changes of the contact area and the shear stress for secondary surface at depth r'_b , b Corresponding permanent shear strain increment AE during rolling forward



to constant stress. From point B to point C, the element is elastically unloaded and deforms in the opposite direction until the yield point D' is reached. The reverse plastic deformation occurs until the maximum normal strain is reached at point D, and then it is unloaded at point E until there is no stress. As the plastic shear of outlet point D exceeds that of inlet point B, the permanent shear strain AE is formed under the contact sub-surface. Due to the existence of internal friction during the loading cycle, the energy loss caused by the elastic hysteresis of the material is amplified. For the reciprocating movement of the ball screw, the continuous shear stress–strain cycle as shown in Fig. 6b repeatedly occurs in the forward and backward movement. Using Eq. (17) and the hysteresis friction coefficient μ_{hs} , the elastic hysteresis friction of a single ball can be obtained as follows:

$$\begin{cases} F_{hs,i}(x_i, y_i) = \frac{3\mu_{hs}Q_i}{2\pi a_i b_i r'_b} \int_{-a_i}^{a_i} \int_0^{b_i \sqrt{1-x_i^2/a_i^2}} \left(1 - \frac{x_i^2}{a_i^2} - \frac{y_i^2}{b_i^2}\right) y_i dy dx_i = \frac{3\mu_{hs}Q_i b_i}{16r'_b} \\ r'_b = \left[R^2 - (c_i a_i)^2\right]^{1/2} - (R^2 - a_i^2)^{1/2} + \left[(d_b/2)^2 - a_i^2\right]^{1/2} \end{cases} \quad (18)$$

where R is the principal curvature radius of the contact deformed pressure surface, $R = 2fd_f/(2f + 1)$, f is the curvature ratio of contact point, the elastic hysteresis friction coefficient $\mu_{hs} = 0.01$ [7]. Therefore, the total elastic hysteretic friction of the ball screw can be expressed as:

$$F_{hs} = \frac{3\mu_{hs}}{16r'_b} \sum_{i=1}^Z Q_i b_i \quad (19)$$

$$F_{s,i}(x_i, y_i) = \frac{3\mu_s Q_i}{2\pi a_i b_i} \left\{ \int_0^{c_i a_i} \int_{-b_i \sqrt{1-x_i^2/a_i^2}}^{+b_i \sqrt{1-x_i^2/a_i^2}} \sqrt{1 - \frac{x_i^2}{a_i^2} - \frac{y_i^2}{b_i^2}} dy_i dx_i - \int_{c_i a_i}^{a_i} \int_{-b_i \sqrt{1-x_i^2/a_i^2}}^{+b_i \sqrt{1-x_i^2/a_i^2}} \sqrt{1 - \frac{x_i^2}{a_i^2} - \frac{y_i^2}{b_i^2}} dy_i dx_i \right\} = \mu_s Q_i (1 + c_i^3 - 3c_i) \quad (21)$$

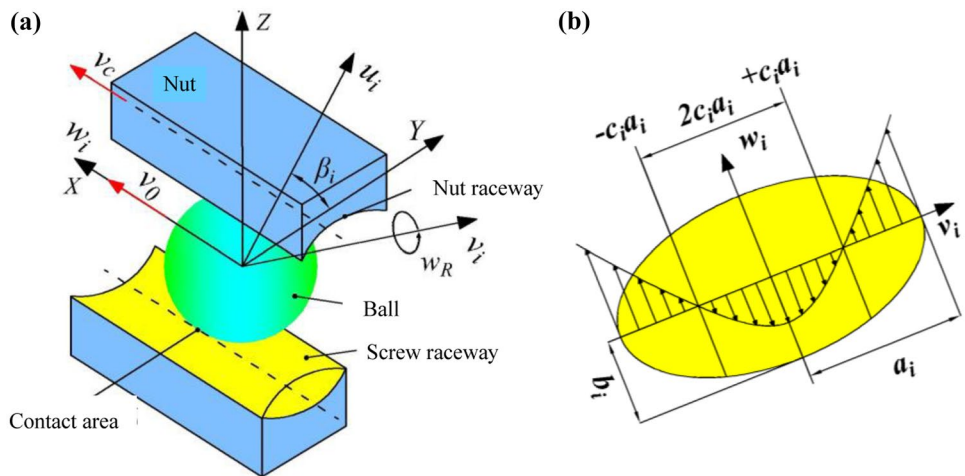
3.3 Analysis of slipping friction force

Figure 7a shows the relative motion state between the ball and the raceway. When the nut moves along the screw axis at the velocity v_c , the ball moves along the raceway around the axis v_i at the angular velocity w_R . Because the distances from the rotation axis of the ball to each point on the contact area are different, the relevant peripheral velocities on the contact area are different. The pure rolling of the ball occurs along the direction of the raceway $v_i = c_i a_i$. The sliding friction due to differential slip is caused by the difference in surface velocity between the raceway and the ball with respect to the axis of rotation v_i , as shown in Fig. 7b. The sliding motion opposite to the rolling direction occurs in the middle region of the contact ellipse, $-c_i a_i < v_i < c_i a_i$, and the sliding region is flanked by the rolling region. According to Eq. (17), the shear stress on the contact surface caused by the slip effect and the contact load can be written as:

$$\tau_{s,i}(x_i, y_i) = \frac{3\mu_s Q_i}{2\pi a_i b_i} \sqrt{1 - \frac{x_i^2}{a_i^2} - \frac{y_i^2}{b_i^2}} \quad (20)$$

The sliding friction coefficient μ_s is 0.15 [7]. By integrating the Hertz contact area, the sliding friction force of the contact area in the rolling contact process can be written as:

Fig. 7 a Relative motion state of contact area. b Slip motion caused by differential slip in the contact area



where $c_i = a_i^2 / (6d_b)$, and the total slip friction caused by differential friction at the contact point can be written as:

$$F_s = \mu_s \sum_{i=1}^Z Q_i (1 + c_i^3 - 3c_i) \quad (22)$$

3.4 Analysis of total friction torque

According to the above analysis of the viscous friction, the elastic hysteretic friction, and the sliding friction of all balls, the friction torque of a single nut under the action of preload can be expressed as:

$$T_P = (F_v + F_{hs} + F_s) \cdot \cos \lambda \cdot R_{AZ} \quad (23)$$

where R_{AZ} is the friction radius of the contact point relative to the screw axis, as shown in Fig. 8. For the double-nut ball screw in the paper, the friction torque can be expressed as:

$$T_N = 2 \cdot T_P = 2 \cdot (F_v + F_{hs} + F_s) \cdot (r_m + r_b \cos \beta_i) \cdot \cos \lambda \quad (24)$$

The friction torque of the double-nut ball screw is calculated by using MATLAB. The algorithm design flow chart is shown in Fig. 9.

4 Experimental details

4.1 The test bench for ball screw

The measurement system of friction torque for the ball screw developed is shown in Fig. 10. When the servo motor drives the screw to rotate, the worktable moves in a straight line at the same speed with the nut. The product of the resistance measured by the sensor and the distance between the bolt and the screw axis is the no-load friction torque

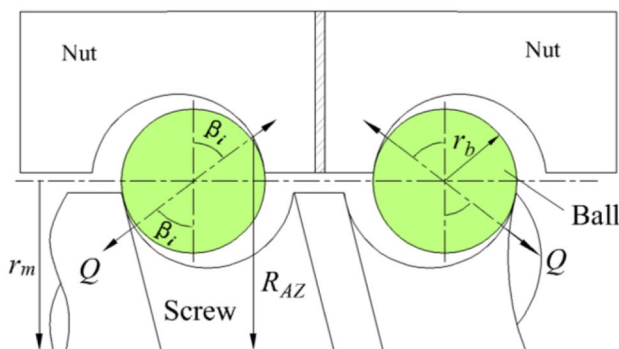


Fig. 8 Friction radius of the ball screw

of the ball screw. The preload double-nut ball screw measured in the paper is GD4008-3 of BT Company, and the diameter of the corresponding standard ball is 4.763 mm. However, the diameter of the ball in the assembly process is 4.759 mm, which avoids interference contact between the ball and the raceway and ensure that the initial preload between the main and auxiliary nuts is zero. The ball screw should be fully lubricated by idling for 10 min before measurement (using ISO VG100 lubricating oil with viscosity grade according to DIN ISO3408-3:2006 measurement conditions).

4.2 Model validation

Taking the ball screw GD4008-3 of BT Company as an example, the structure parameters and the lubrication parameters are shown in Table 1.

Figure 11 shows the positive and negative friction torque and the mean friction torque in different position of the ball screw with the rotational speed 100 rpm and six kinds of preload. Due to the impact of the travel error for the ball screw, the friction torque is different in different positions. Therefore, the nominal friction torque of the ball screw is actually the average value of the effective friction torque in the stroke. (In Fig. 11, 1–6 KN represents the preload of the ball screw, and the actual mean values of friction torque at different preload are 0.409 N. mm, 0.828 N. mm, 1.168 N. mm, 1.542 N. mm, 1.889 N. mm, and 2.224 N. mm respectively). It can be seen from Fig. 11 that the friction torque in the front 600 mm stroke of the ball screw is lower than the mean friction torque at the same preload and it is opposite in the back 600 mm stroke, which is caused by the manufacturing taper of the ball screw. The runout of friction torque decreases with the increasing preload, because the higher preload can improve the stiffness of the ball screw and reduce friction vibration.

Figure 12 shows the theoretical and experimental values of friction torque under different preload (100 rpm). The calculation model of friction torque proposed in the paper, which the ball load distribution and thermal elastohydrodynamic lubrication is considered, is in good agreement with the test value. However, the deviation between the calculated value of Zhou et al. [26] model and the test value increases with the increase of preload, which is mainly because the contact load of all balls in Zhou model are assumed to be consistent. However, the larger preload lead to the greater difference of the contact load for all balls, and the lubrication performance of each ball is different under different contact load. Moreover, the calculation value based on the empirical formula proposed by NSK Company has a large deviation compared with the experimental value, and the empirical

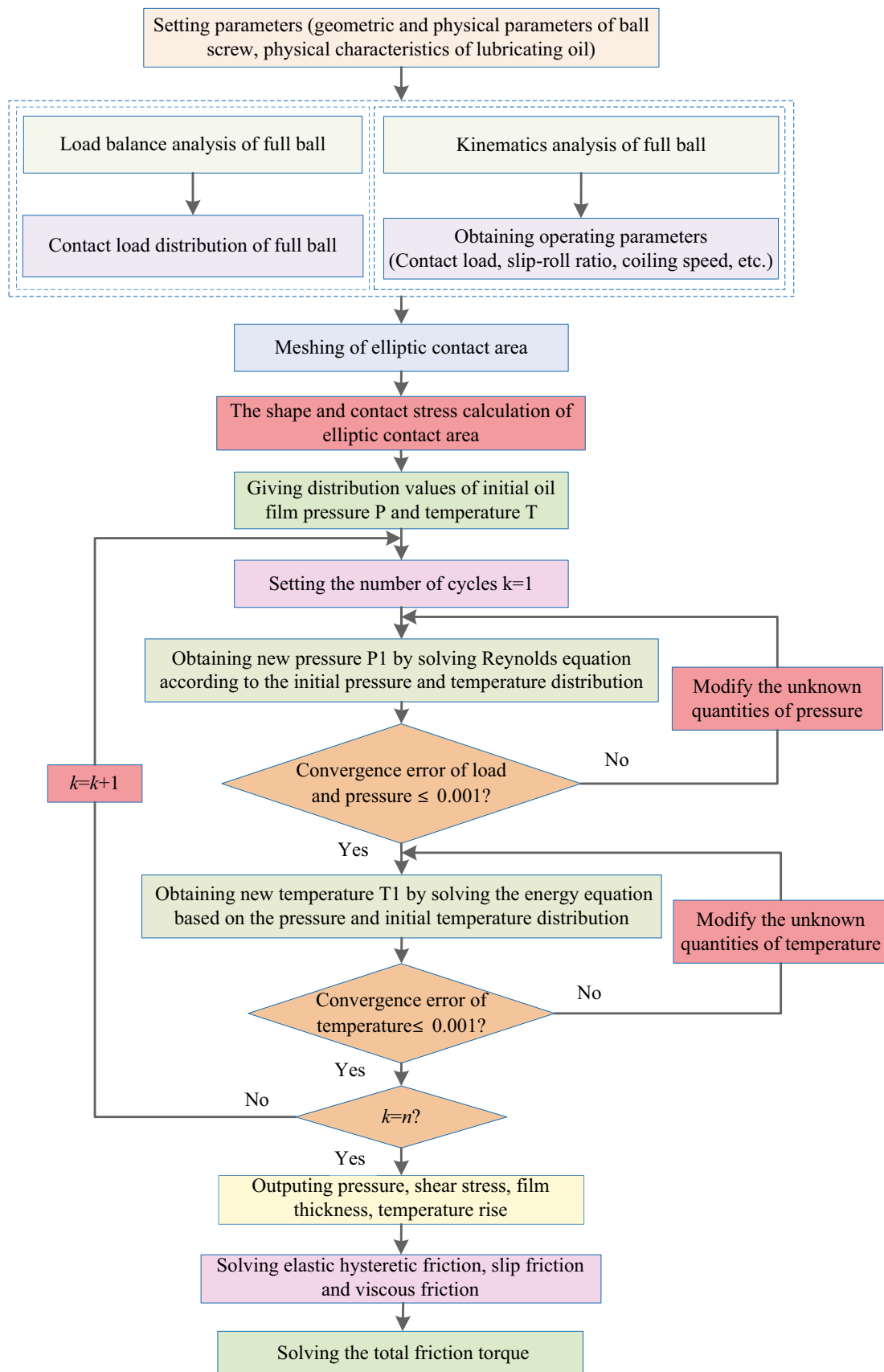
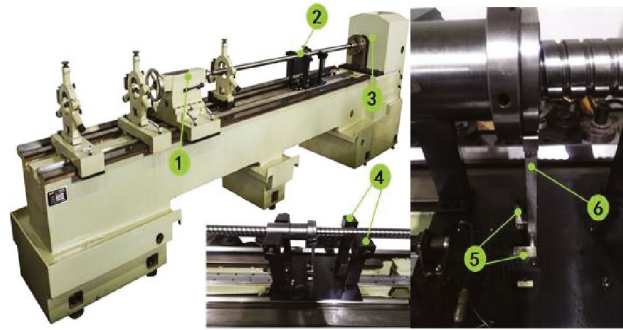


Fig. 9 Algorithm design flow chart of friction torque

Fig. 10 Measuring test bench of friction torque for ball screw. 1-tailstock; 2-ball screw; 3-headstock; 4-support device; 5-pressure sensor; 6-driving lever



1-Tailstock; 2-Ball screw; 3-Headstock; 4-Support device; 5- Pressure sensor; 6-Driving lever.

formula of friction torque proposed by NSK Company can be expressed as $T_p = 0.05 \cdot F_p \cdot L_p / (2\pi \cdot \sqrt{\tan \lambda})$ [24]. The empirical formula is based on the principle of energy conversion. The work of friction torque ($T_p \cdot 2\pi$) is equal to the work of preload ($F_p \cdot L_p$) multiplied by the coefficient ($0.05/\sqrt{\tan \lambda}$). The preload of the ball screw is internal force and is not actually doing work, which results in a large error compared with the experimental value.

According to the measurement conditions specified in the international standard DIN ISO3408-3:2006, the relative error between the test value and the no-load friction torque calculated by using Eq. (24), Zhou et al. [26] and the model proposed in NSK is shown in Table 2. It can be seen from Table 2 that the average deviation between the no-load friction torque calculated by Eq. (24) and the test value is 1.59% at the preload of 1–6kN. However, the average deviation between the test value and the no-load friction torque calculated by Zhou et al. [26] and NSK model is 4.15% and 34.34%, respectively. It can be seen that the reference preload with the theoretical value calculated by Eq. (24), Zhou et al. [26] and NSK model in the case of known no-load torque is compared in Table 3. Similar to Table 2, the average deviation between the theoretical preload calculated by Eq. (24) and the benchmark value is 2.19% at the preload of 1–6kN. However, the average deviation of the theoretical preload in Zhou et al. [26] is 4.57% compared with the experimental value under six kinds of no-load friction torque. The prediction deviation of the preload increases with the increase of friction torque. The theoretical value calculated by NSK model has a large deviation (above 46.85% and greater than the benchmark value).

Figure 13 shows the positive and negative friction torque and the mean friction torque at different position of ball screw under the preload of 1000 N and six kinds of speed. (In Fig. 13, 100 r/min, 500 r/min, 1000 r/min, 1500 r/min, 2000 r/min, and 2500 r/min represent the speed of the ball screw, and the actual mean friction torques at different speed are 0.409 N. mm, 0.612 N. mm, 0.682 N. mm, 0.748 N. mm, 0.802 N. mm, and 0.846 N. mm respectively). It can

be seen from Fig. 13 that the friction torque of the ball screw increases with the increasing rotational speed, and the runout of friction torque decreases gradually at high rotational speed. The lubricating oil film is easy to be formed at high rotational speed, so that the contact point of the ball is fully lubricated.

Figure 14 shows the theoretical and experimental friction torque for the ball screw at different speed and the preload 1000 N. The calculated value of the friction torque model proposed in the paper is in good agreement with the experimental friction torque, but the calculated value of the Zhou model and NSK model is unchanged with the increase speed of the ball screw (the influence of the speed on the friction torque is ignored). The comparison of friction torque test value and model calculated value at different speed is shown in Table 4. Therefore, it can be known that the average deviation of friction torque calculated by Eq. (24) compared with the test value is 1.59% at different speeds of 100 r/min, 500 r/min, 1000 r/min, 1500 r/min, 2000 r/min, and 2500 r/min. As shown in Fig. 14, the average deviation of friction torque calculated by Zhou model and NSK model gradually increases with the increase of rotational speed, and the deviation of friction torque in NSK model is larger than that in Zhou model.

It can be seen from Fig. 15 that the mean frictional torque for the positive and negative stroke gradually increases with the increasing rotational speed when the preload is low. The friction torque is increasingly affected by rotational speed with the increasing preload, and the frictional torque at different rotational speed gradually shows a stable state. The main reason for the phenomenon is that the pressure of contact point is small when the preload is low, and the oil film is not easy to be formed. The lubrication between the ball and the raceway gradually deteriorates with the increase of the speed, which causes that the friction torque increases continuously. When the preload is high, the pressure between the ball and the raceway is large and the lubricating oil film is easy to be formed. Therefore, it is always in a good lubrication state at different speed, so the friction torque is stable.

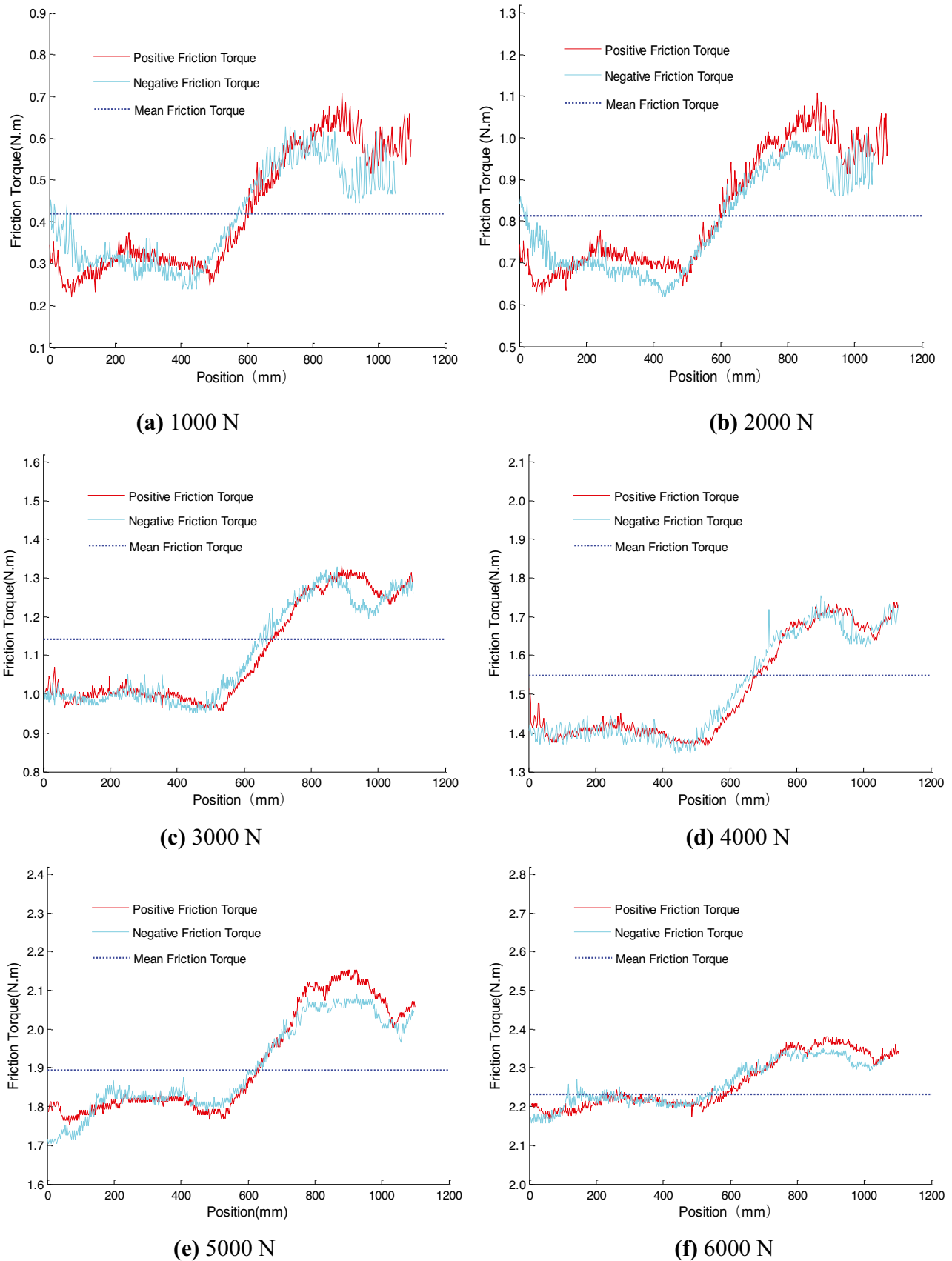


Fig. 11 Change of friction torque with position under different preload. **a** 1000 N, **b** 2000 N, **c** 3000 N, **d** 4000 N, **e** 5000 N, **f** 6000 N

Fig. 12 Theoretical and experimental values of friction torque under different preload (100 rpm)

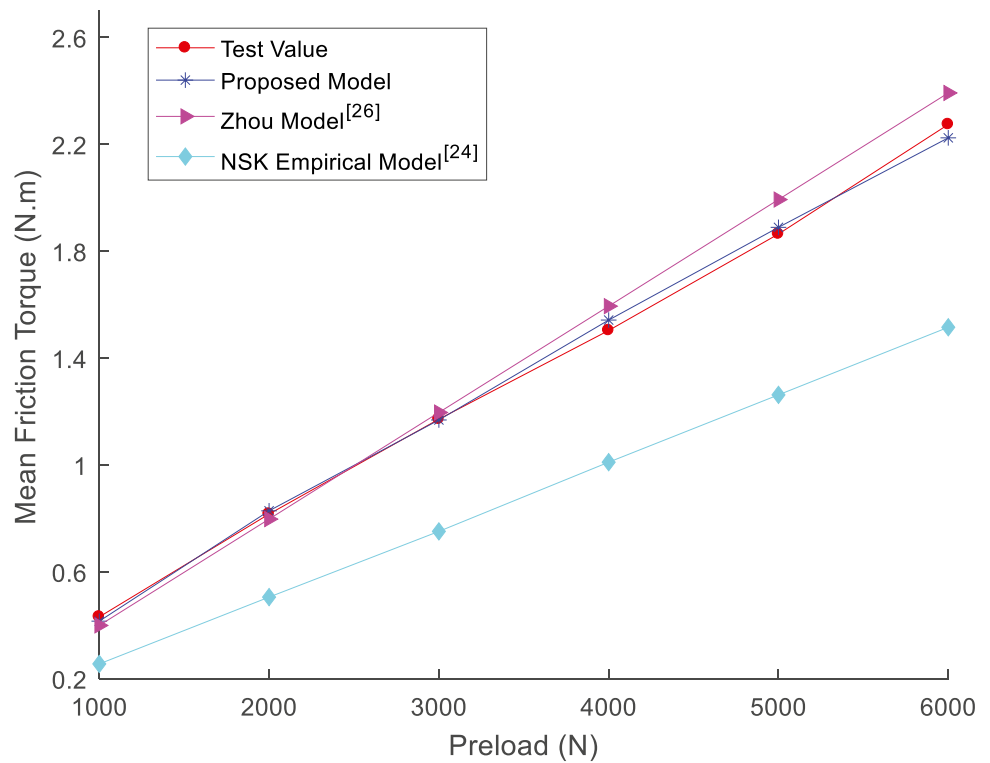


Table 2 Comparison between the experimental friction torque under the measurement conditions specified in international standard and the calculated value of the model

Friction torque (N. m)	Preload (N)	Proposed model		Zhou model [26]		NSK model [24]	
		Data (N. m)	Relative error	Data (N. m)	Relative error	Data (N. m)	Relative error
0.409	1000	0.416	1.71%	0.399	2.45%	0.255	37.65%
0.828	2000	0.816	1.45%	0.805	2.77%	0.505	39.00%
1.168	3000	1.171	0.25%	1.206	3.26%	0.751	35.70%
1.542	4000	1.503	2.53%	1.594	3.37%	1.010	28.60%
1.889	5000	1.864	1.32%	1.993	5.51%	1.262	33.19%
2.224	6000	2.274	2.25%	2.392	7.56%	1.515	31.87%

Table 3 Comparison between the test value of preload and the theoretical value of the model under the measurement conditions specified in international standard

Friction torque (N. m)	Standard preload (N)	Proposed model		Zhou model [26]		NSK model [24]	
		Data (N)	Relative error	Data (N)	Relative error	Data (N)	Relative error
0.409	1000	1020.6	2.06%	1025.9	2.59%	1620.4	62.04%
0.828	2000	2054.8	2.74%	2077.0	3.85%	3280.4	64.02%
1.168	3000	2939.2	2.03%	2875.9	4.14%	4627.5	54.25%
1.542	4000	3918.0	2.05%	3818.0	4.55%	6109.2	52.73%
1.889	5000	4856.4	2.87%	4738.4	5.23%	7484.0	49.68%
2.224	6000	5916.5	1.39%	5578.8	7.02%	8811.2	46.85%

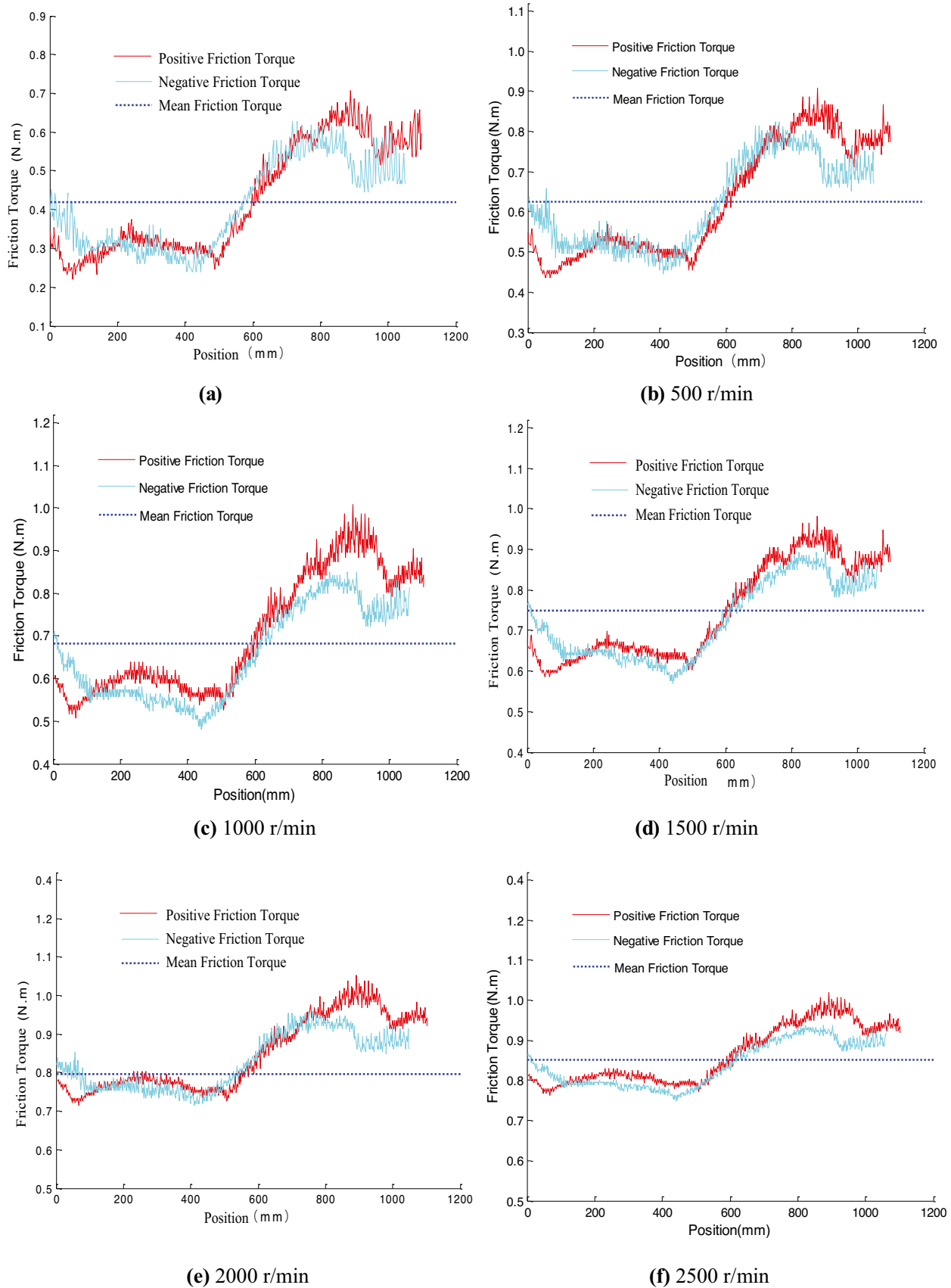


Fig. 13 Change of friction torque with position at different rotational speed. a 100 r/min, b 500 r/min, c 1000 r/min, d 1500 r/min, e 2000 r/min, f 2500 r/min

Fig. 14 Comparison between theoretical and experimental values of friction torque at different speed

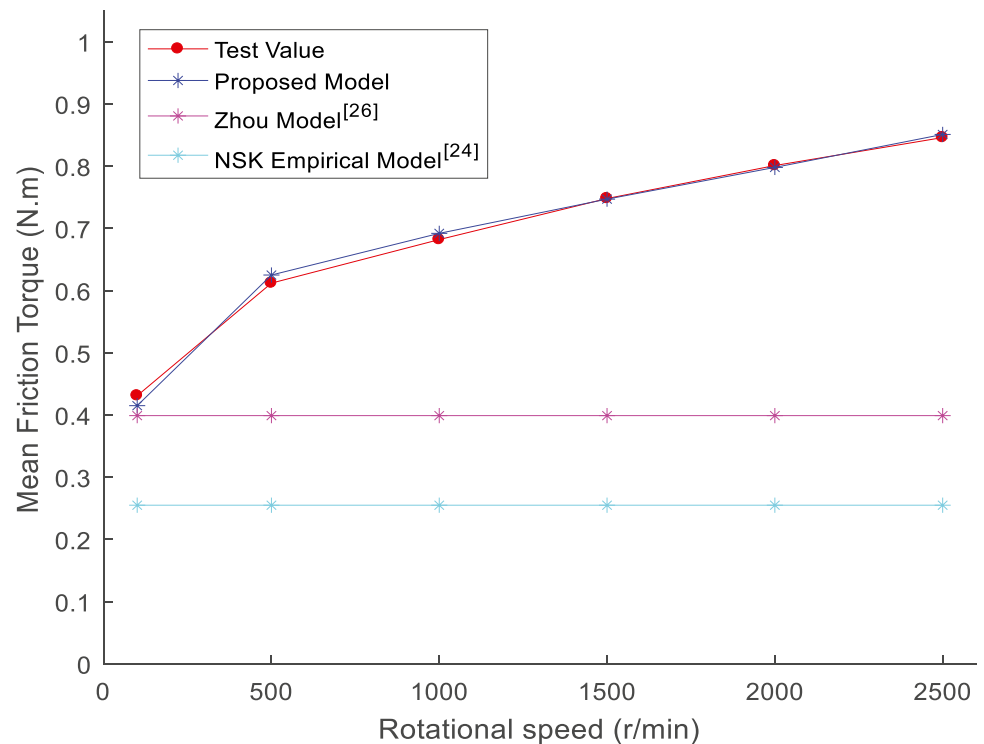


Figure 16 shows the change of friction coefficient for the ball screw with rotational speed under different preload, which is similar to the change trend of friction torque in Fig. 15. For given a certain preload, the friction coefficient increases with the increase of the screw speed. The greater the preload is, the less the influence of rotation speed on friction coefficient is. When the preload changes from 1 to 6 KN, the friction coefficient of the ball screw varies from 0.0056 to 0.0065 at low speed (100 r/min). The friction coefficient varies from 0.0095 to 0.0127 at high speed (2500 r/min). The friction coefficient corresponding to different preload increases and the variation gradually increases with the increase of speed, which indicates that it is reasonable to set the measurement speed of no-load friction torque for the ball screw as 100 r/min in the international standard DIN ISO3408-3:2006.

5 Results and discussion

5.1 Thermal elastohydrodynamic lubrication analysis of a single ball

Keep the preload of the ball screw at 2000 N and rotational speed at 3000 r/min. Based on the analysis of all ball load distribution for the ball screw [2, 3], the initial contact load between the ball and the raceway is obtained to be 39.5 N. According to the above kinematic analysis, the initial slide-roll ratio between the ball and the screw raceway is 0.63174, and the coiling speed is 4374.37 mm/s. The sliding ratio between the ball and the nut raceway is 1.94203, and the coiling speed is 1541.64 mm/s. Figures 17 and 18 show the regional distribution of contact stress, shear stress, film thickness, and temperature rise for the

Table 4 Comparison between experimental friction torque at different speed and calculated value of the model

Friction torque (N. m)	Speed (r/min)	Proposed model		Zhou model [26]		NSK model [24]	
		Data (N. m)	Relative error	Data (N)	Relative error	Data (N)	Relative error
0.409	100	0.418	1.71%	0.399	2.45%	0.255	37.65%
0.612	500	0.625	2.13%	0.399	34.80%	0.255	58.33%
0.682	1000	0.692	1.47%	0.399	41.50%	0.255	62.61%
0.748	1500	0.747	0.14%	0.399	46.66%	0.255	65.91%
0.802	2000	0.798	0.50%	0.399	50.25%	0.255	68.21%
0.846	2500	0.851	0.61%	0.399	52.84%	0.255	69.86%

Fig. 15 Change of mean friction torque at different rotational speed

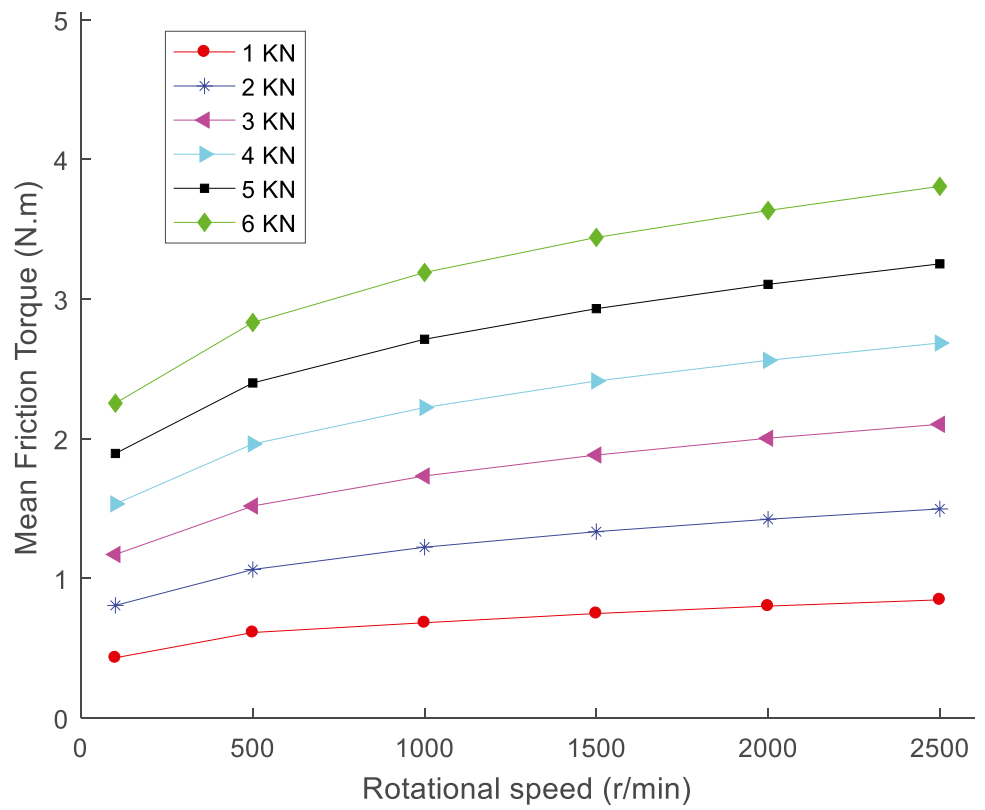
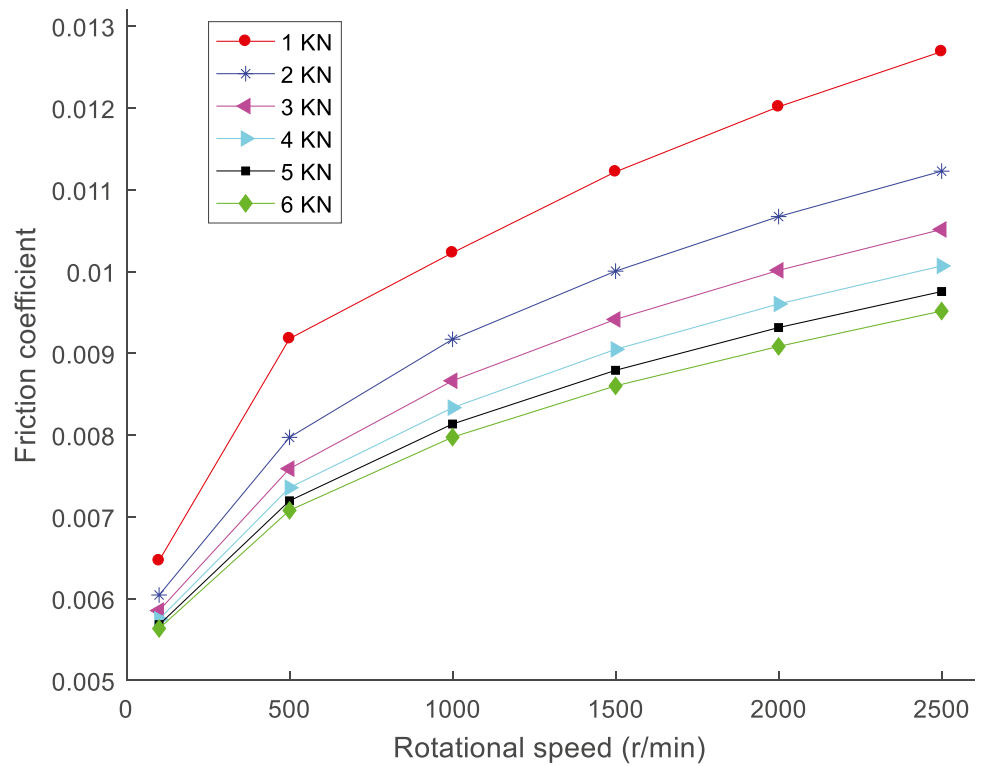


Fig. 16 Change of friction coefficient at different rotational speed



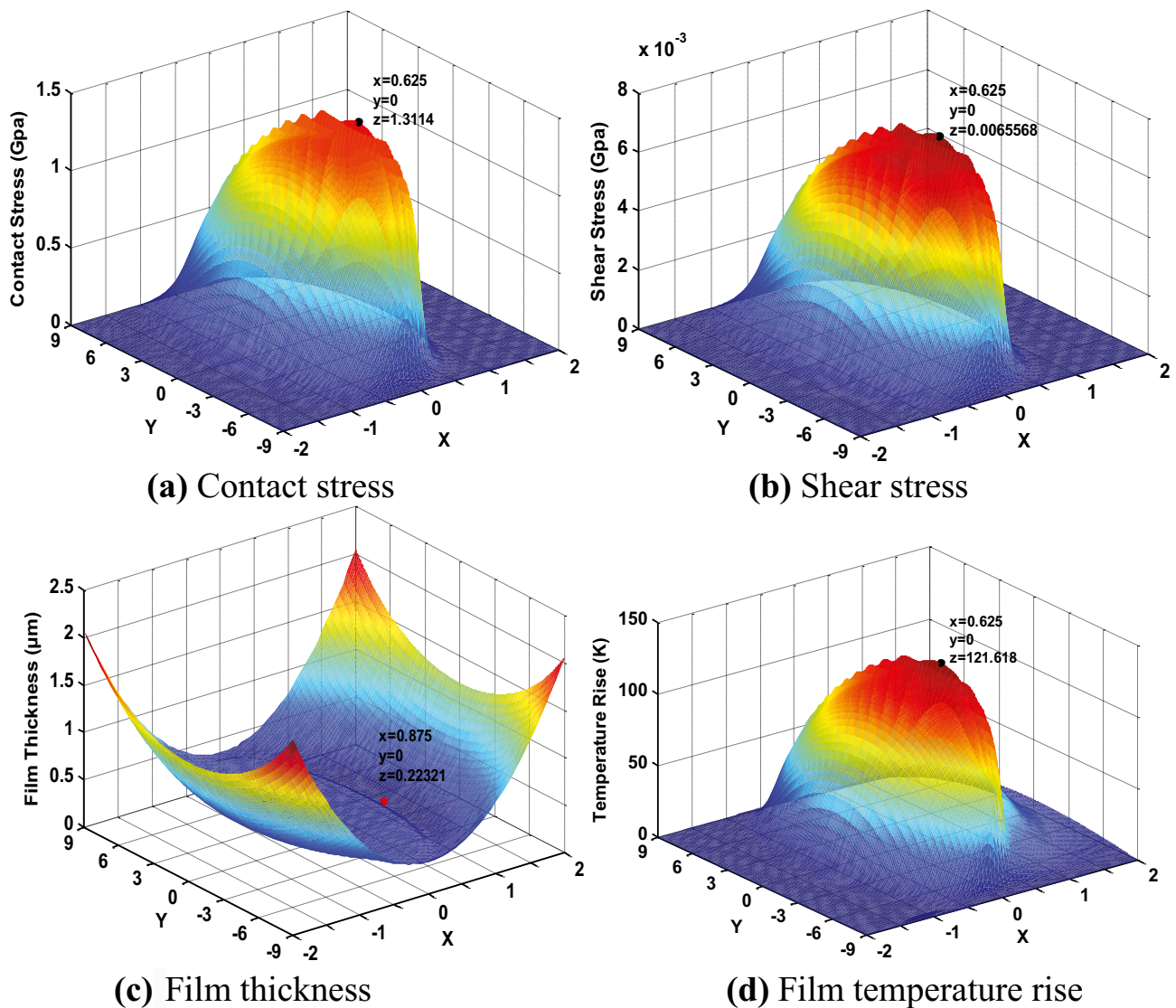


Fig. 17 Lubrication performance of contact point between ball and screw raceway. **a** contact stress, **b** shear stress, **c** film thickness, **d** film temperature rise

contact points of the screw raceway and the nut raceway respectively. The maximum contact stress and the maximum shear stress of contact point for the screw raceway are larger than that of contact point for the nut raceway, which is caused by the smaller contact curvature of the ellipse contact point for the screw raceway. The minimum film thickness of contact point for the screw raceway is more than two times larger than that of contact point for the nut raceway, and the minimum film thickness is only $0.223 \mu\text{m}$. It can be seen that the oil film thickness formed at high speed is small, while the oil film thickness formed at low speed is smaller. Therefore, the ball screw is easy to be affected by the insufficient lubrication, resulting in the increased friction. The maximum temperature rise of

oil film at contact point of the screw raceway is 121.62 K , which is 10 K higher than the contact point of the nut raceway. It can be seen that the teeth of the screw are more likely to fail than the teeth of the nut due to the influence of high temperature adhesion.

5.2 Analysis of friction torque at different rotational speed

The preload of the ball screw is kept at 1800 N , and the friction torque of the ball screw at different speed is shown in Fig. 19. Since the elastic hysteretic friction torque term and the sliding friction torque term are composed of preload, geometric information, elastic hysteretic friction

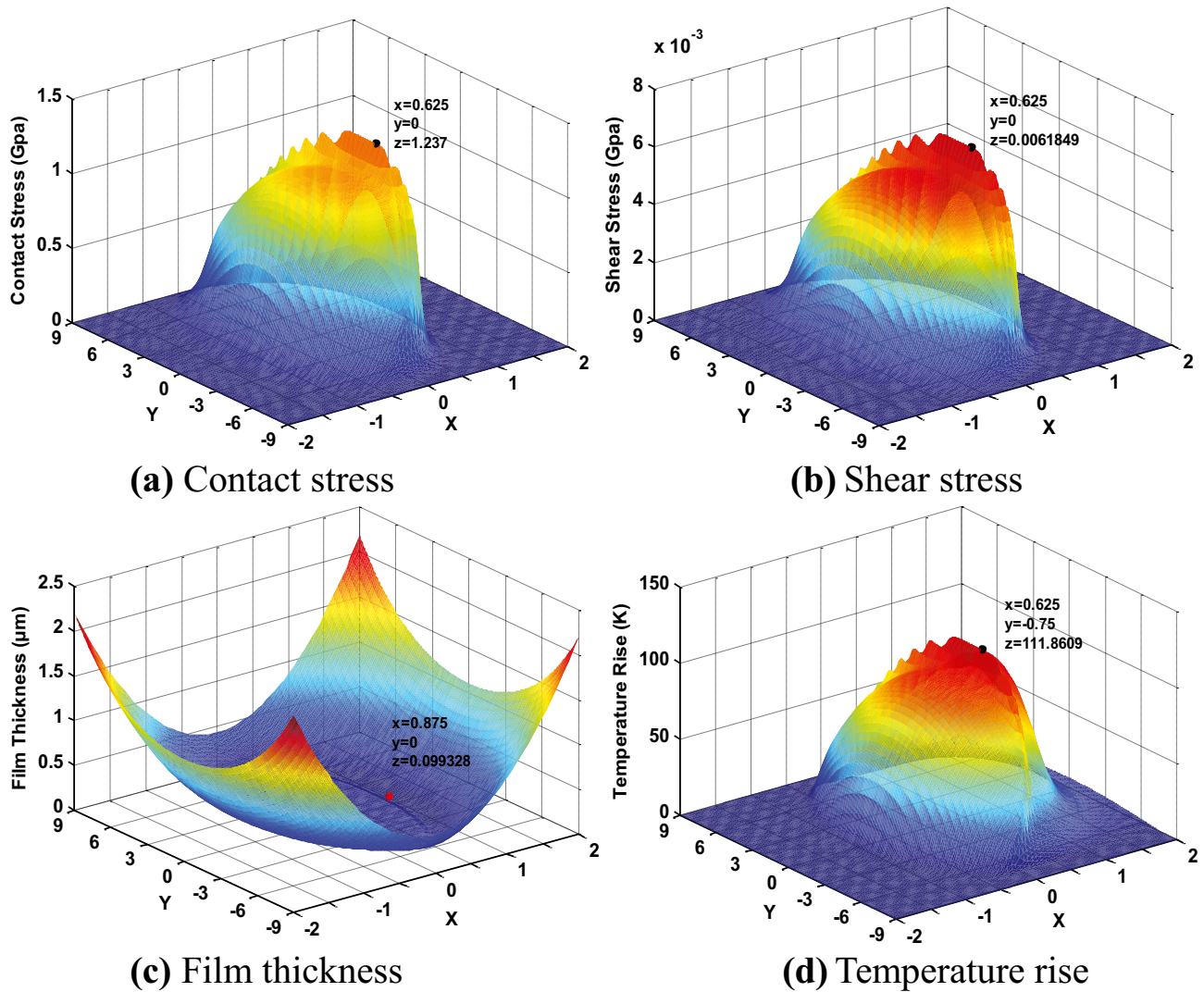


Fig. 18 Lubrication performance of contact point between ball and nut raceway. **a** Contact stress, **b** shear stress, **c** film thickness, **d** temperature rise

coefficient, and rolling friction coefficient, these will keep constant value when the speed of the screw changes. The sliding friction term has a higher influence than the elastic hysteresis friction term. The viscous friction term depends on the contact ellipse radius caused by the contact load of the ball, the oil film thickness, the viscosity of lubricant, etc. Therefore, the viscous friction term increases with the increase of the screw speed. Obviously, the elastic hysteresis friction torque is relatively small in the beginning. When the rotational speed of the ball screw is less than 186 r/min, the sliding friction torque generated by the contact load of the ball is higher than the viscous friction torque. The viscous friction torque plays a predominant role when the screw is at a high rotation speed, which causes the total friction torque of the ball screw increases with the increase of rotational speed.

5.3 Analysis of sliding coefficient and environment temperature

Figures 20 and 21 show the friction torque under different sliding friction coefficients and the change of friction torque under different environment viscosity caused by different lubricating oil temperature obtained from Eqs. (19) and (22) respectively. The friction torque of the ball screw is nonlinear with the change of the screw speed. The friction torque increases with the increase of sliding friction coefficient and the increase of initial environment temperature. When the environmental viscosity of lubricating oil increases by 0.025 Ns/m^2 , the friction torque increases by 6.4% on average. When the sliding friction coefficient increases by 0.001, the friction torque increases by 9.9% on average.

Fig. 19 Friction torque at different speed

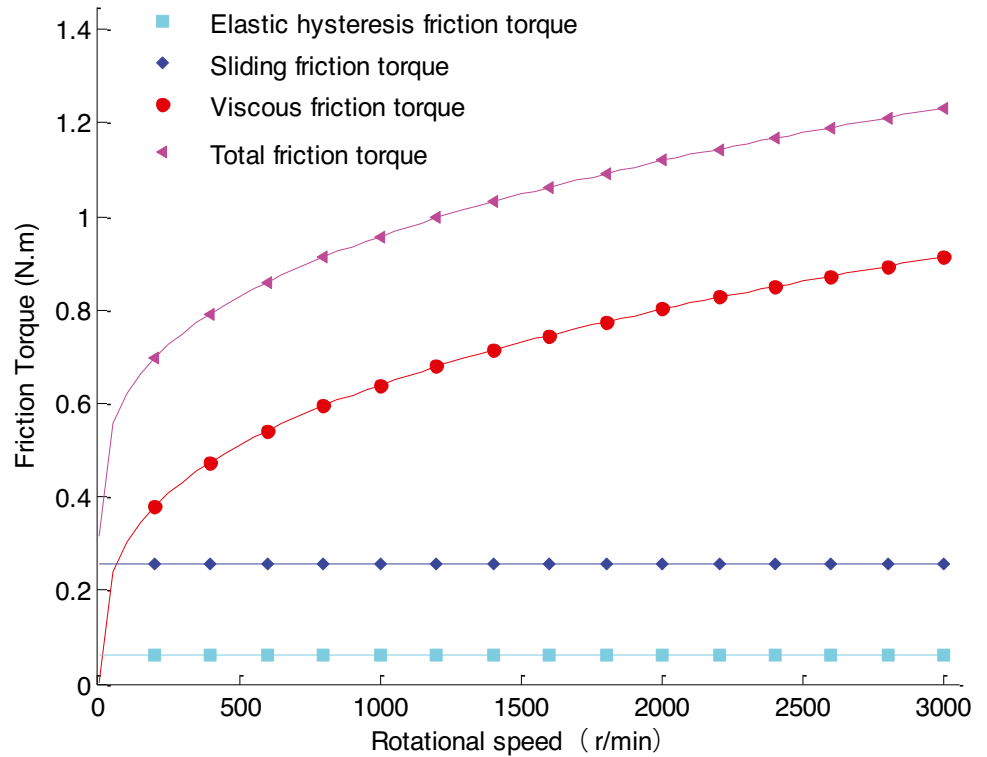


Fig. 20 Friction torque under different sliding friction coefficient

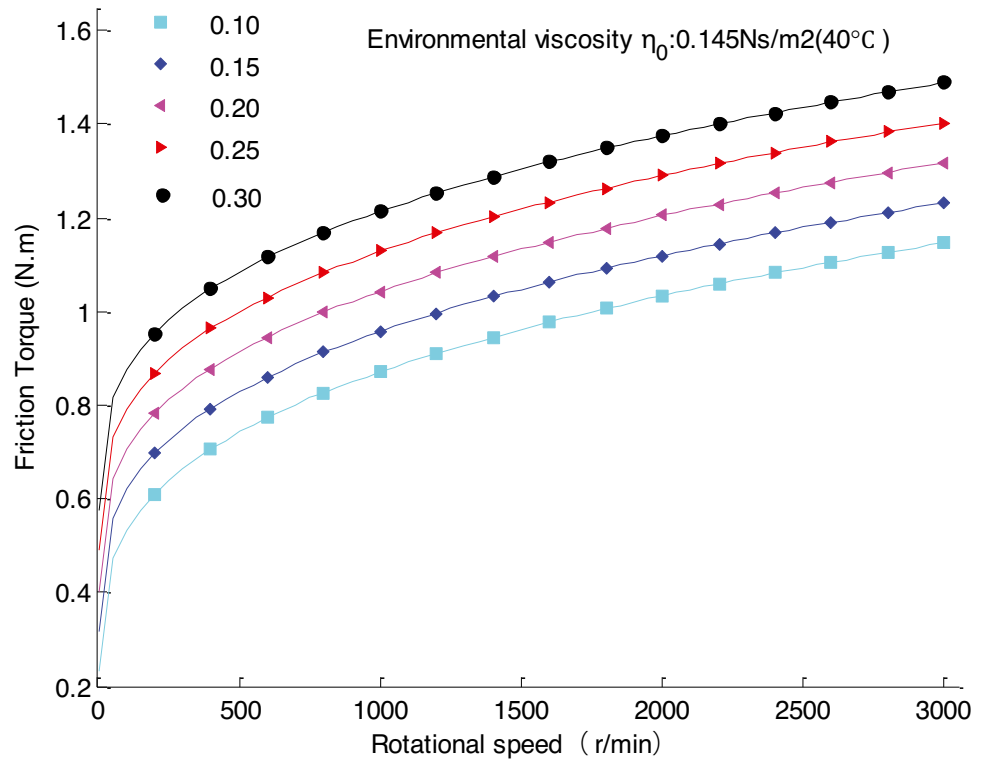
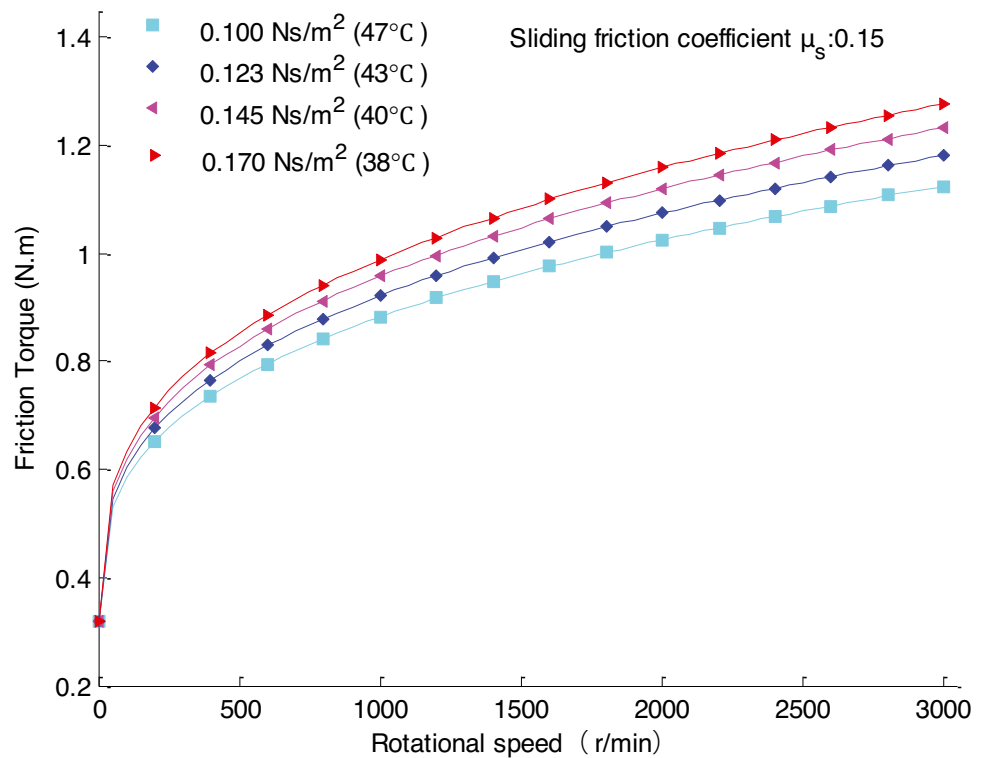


Fig. 21 Friction torque at different environmental viscosity

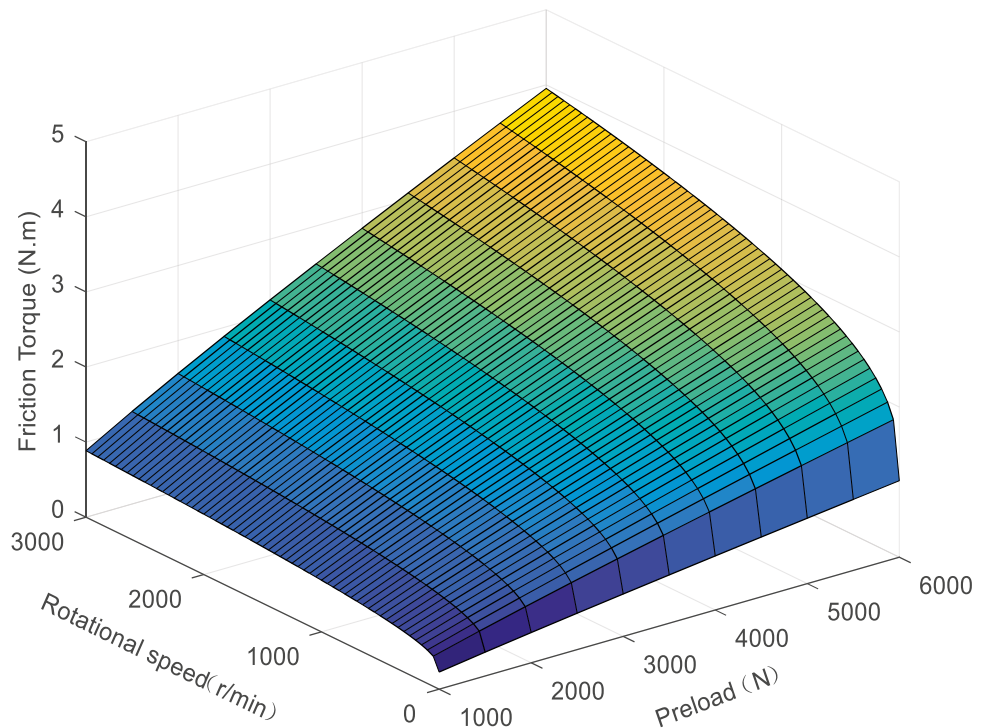


5.4 Analysis of friction torque with the screw speed and preload

Figure 22 shows the change trend of friction torque for the ball screw with the change of the screw speed and the preload. It can be obviously seen that the friction torque

increases with the increase of the preload and the screw speed. The friction torque changes greatly with the increase of speed at low speed, which is caused by the large change rate of the viscous friction for the ball screw. When running at high speed, the change of friction torque is relatively stable, and the change rate of viscous friction torque is no

Fig. 22 Change of friction torque with the screw speed and preload



longer obvious because the film thickness of contact lubricating oil has been formed. For a given constant preload, the friction torque increases by 0.12 N·m on average when the screw speed increases by 1000 r/min. For a given constant speed, the relationship between the friction torque and the preload is close to linear, and the friction torque increases by 0.65 N·m on average when the preload increases by 1000 N.

6 Conclusion

The coupling analysis model of thermal elastohydrodynamic lubrication and operation of the ball screw is established in the paper. Based on the Reynolds equation considering the influence of temperature rise, the lubrication performance of the contact point is studied. The failure area caused by insufficient lubrication is analyzed by comparing the oil film pressure, shear stress, film thickness, and temperature rise of the contact point for the screw and nut raceway. On this basis, the ball load distribution of the double-nut ball screw is analyzed under the action of the preload, and the calculation method of friction torque for the ball screw considering the viscous friction, the elastic hysteresis friction, and the sliding friction is put forward. The calculation accuracy of friction torque considering the ball load distribution and the thermal elastohydrodynamic lubrication is verified by experiments. The main conclusions can be expressed as follows:

1. The calculated value of the friction torque model considering the viscous friction, elastic hysteretic friction, and sliding friction is in good agreement with the experimental value, and the viscous friction torque term increases with the increase of the screw speed. When the speed of the ball screw is below 186 r/min, the sliding friction torque generated by the contact load of the ball is higher than the viscous friction torque, and the viscous friction torque plays a dominant role in the high-speed rotation of the ball screw, resulting in the increase of the total friction torque with the increase of the speed.
2. When the preload is low, the mean friction torque for the positive and negative stroke increases gradually with the increase of rotational speed. The friction torque is more seriously influenced by rotational speed with the increase of preload, and the friction torque at different rotational speed gradually presents a stable state. When the preload is high, the contact pressure between the ball and the raceway is large, and the oil film is easy to be formed. Therefore, it is always in a good lubrication state, and the friction torque is stable.
3. When the preload changes from 1 to 6kN, the friction coefficient of the ball screw varies from 0.0056 to 0.0065 at low speed (100 r/min). The friction coefficient

varies from 0.0095 to 0.0127 at high speed (2500 r/min). The variation of the friction coefficient increases gradually with the increase of rotational speed, which indicates that it is reasonable to set the measurement speed of no-load friction torque of ball screw as 100 r/min in the international standard DIN ISO3408-3:2006.

Author contribution JZ and BQ are responsible for providing overall research ideas. XS, HJ, and PD are responsible for the measurement of friction torque for ball screw. JZ and XS are responsible for experimental data analysis.

Funding This work was supported by the National Natural Science Foundation of China (grant no.51475267) and Natural Science Foundation of Shandong Province (grant no. ZR2020ME117, ZR2020ME166).

Availability of data and materials Not applicable.

Declarations

Ethics approval Not applicable.

Consent to participate Not applicable.

Consent to publish Not applicable.

Conflict of interest The authors declare no competing interests.

References

1. Shi H, Ma C, Yang J (2015) Investigation into effect of thermal expansion on thermally induced error of ball screw feed drive system of precision machine tools. *Int J Mach Tools Manuf* 97:60–71
2. Zhao JJ, Lin MX, Song XC, Wei N (2021) A modeling method for predicting the precision loss of the preload double-nut ball screw induced by raceway wear based on fractal theory. *Wear* 486–487:204065
3. Zhao JJ, Lin MX, Song XC, Guo QZ (2019) Investigation of load distribution and deformations for ball screws with the effects of turning torque and geometric errors. *Mech Mach Theory* 141:95–116
4. Cheng Q, Qi BB, Liu ZF, Zhang CX, Xue DY (2019) An accuracy degradation analysis of ball screw mechanism considering time-varying motion and loading working conditions. *Mech Mach Theory* 134:1–23
5. Kwang-Je Oh, Khim G, Park C-H, Chung S-C (2019) Explicit modeling and investigation of friction forces in linear motion ball guides. *Tribol Int* 129:16–28
6. Cao L, Oh KJ, Chung SC (2020) Explicit precision friction torque model of ball screws in high speed operations. *Tribol Int* 152:106573
7. Oh KJ, Cao L, Chung SC (2020) Explicit modeling and investigation of friction torques in double-nut ball screws for the precision design of ball screw feed drives. *Tribol Int* 141:105841
8. Wang Q, Lin MX (2016) Electromechanical coupling measurement of a new giant magnetostrictive structure for double-nut ball screw pre-tightening. *Meas Sci Technol* 27(12):125906
9. Lin MC, Ravani B, Velinsky SA (1994) Kinematics of the ball screw mechanism. *J Mech Des* 116(3):849–855
10. Hu JZ, Wang M, Zan T (2014) The kinematics of ball-screw mechanisms via the slide-roll ratio. *Mech Mach Theory* 79:158–172

11. Wei CC, Lai RS (2011) Kinematical analyses and transmission efficiency of a preloaded ball screw operating at high rotational speeds. *Mech Mach Theory* 46(7):880–898
12. Wei CC, Lin JF (2003) Kinematic analysis of the ball screw mechanism considering variable contact angles and elastic deformation. *J Mech Des* 125(4):717–733
13. Okwudire CE, Altıntans Y (2009) Hybrid modeling of ball screw drives with coupled axial, torsional, and lateral dynamics. *J Mech Des* 131:1–9
14. Huang HW, Tsai MS, Huang YC (2018) Modeling and elastic deformation compensation of flexural feed drive system. *Int J Mach Tools Manuf* 132:96–112
15. Yoshich T, Tozak Y, Matsumoto S (2003) Study on load distribution of ball screw. *J Jpn Soc Tribol* 48(8):659–666
16. Yoshida T, Tozaki Y, Kato N, Matsuo S (2007) Study on static load distribution of ball screw with gothic arc groove. *J Jpn Soc Tribol* 52(11):793–800
17. Mei XS, Tsutsumi M, Tao T, Sun N (2003) Study on the load distribution of ball screws with errors. *Mech Mach Theory* 38:1257–1269
18. Xu S, Sun YF, Shen H (2013) Load distribution of ball screw with contact angle variation. *Appl Mech Mater* 397–400:435–440
19. Liu C, Zhao CY, Meng XL, Wen BC (2020) Static load distribution analysis of ball screws with nut position variation. *Mech Mach Theory* 151:103893
20. Zhen N, An Q (2018) Analysis of stress and fatigue life of ball screw with considering the dimension errors of balls. *Int J Mech Sci* 137:68–76
21. Lin B, Okwudire CE (2016) Low-order contact load distribution model for ball nut assemblies. *SAE Int J Passeng Cars Mech Syst* 9:535–540
22. Lin B, Okwudire CE, Wou JS (2018) Low order static load distribution model for ball screw mechanisms including effects of lateral deformation and geometric errors. *J Mech Des* 140:022301
23. Zhou CG, Xie JL, Feng HT (2021) Investigation of the decompression condition of double-nut ball screws considering the influence of the geometry error and additional elastic unit. *Mech Mach Theory* 156:104164
24. SKN (2003) Precision machine components catalogue, NSK, Tokyo
25. Xu NN, Tang WC, Chen YJ, Bao DF, Guo YJ (2015) Modeling analysis and experimental study for the friction of a ball screw. *Mech Mach Theory* 87:57–69
26. Zhou CG, Feng HT, Chen ZT, Ou Y (2016) Correlation between preload and no-load drag torque of ball screws. *Int J Mach Tools Manuf* 102:35–40
27. Bertolino AC, Jacazio G, Mauro S, Sorli M (2021) Investigation on the ball screws no-load drag torque in presence of lubrication through MBD simulations. *Mech Mach Theory* 161:104328
28. Zhao LL, Feng HT, Jin J (2018) A modified ball screw lapping method and optimized lapping factors for ideal surface quality. *Mech Sci* 9:221–230
29. Bertolino AC (2020) High fidelity model of ball screws to support model-based health monitoring. Politecnico di Torino
30. Bertolino AC, Sorli M, Jacazio G, Mauro S (2019) Lumped parameters modelling of the EMAs' ball screw drive with special consideration to ball/grooves interactions to support model-based health monitoring. *Mech Mach Theory* 137:188–210
31. Zhao JJ, Lin MX, Song XC, Guo QZ (2020) Analysis of the precision sustainability of the preload double-nut ball screw with consideration of the raceway wear. *Part J J Eng Tribol* 234(9):1530–1546
32. Zhao JJ, Lin MX, Song XC, Wei N (2020) Coupling analysis of the fatigue life and the TEHL contact behavior of ball screw under the multidirectional load. *IndLubr Tribol* 72(10):1285–1293

Publisher's note Springer Nature remains neutral with regard to jurisdictional claims in published maps and institutional affiliations.